actuators

MDPI

Article

Intermittent Short Circuit Fault Location for CAN Based on Two-Port Network Modeling

Longkai Wang, Yi Yang and Yong Lei *

State Key Laboratory of Fluid Power and Mechatronic Systems, Zhejiang University, Hangzhou 310027, China; lkwang@zju.edu.cn (L.W.); 22025196@zju.edu.cn (Y.Y.)
* Correspondence: ylei@zju.edu.cn

Abstract: The Controller Area Network (CAN) has been adopted in various reliability-critical industrial systems. However, intermittent connection (IC) problems of network cables may worsen system performance and even threaten operational safety. Recently, there have been several studies on diagnosing intermittent open circuit faults, but the intermittent short circuit (ISC) fault diagnosis has not been addressed. In this paper, a novel ISC fault location method for CANs is proposed based on two-port network modeling. First, the CAN network is modeled as a switched system that depends on the states of the sending nodes using a two-port network approach. An equivalent circuit model and a voltage transfer difference function (VTDF) group are derived for each state where one particular node is sending. Second, upon each fault, corresponding direction events are defined by comparing the two VTDF values that are calculated from the voltages collected at network ends. Then, the fault and health domains can be determined by integrating these direction events with the network topology information according to their statistical significance. Third, a bidirectional eviction localization algorithm is developed to identify ISC fault locations based on the fault and health domains. A testbed is constructed, and case studies are conducted to demonstrate that the proposed method can correctly locate the ISC faults in various network topological layouts.

Keywords: controller area network; fault location; intermittent fault; short circuit; two-port network modeling

check for updates

Citation: Wang, L.; Yang, Y.; Lei, Y. Intermittent Short Circuit Fault Location for CAN Based on Two-Port Network Modeling. *Actuators* **2024**, *13*, 485. https://doi.org/10.3390/act13120485

Academic Editor: Anyang Lu

Received: 5 November 2024
Revised: 23 November 2024
Accepted: 27 November 2024
Published: 29 November 2024

Copyright: © 2024 by the authors. Licensee MDPI, Basel, Switzerland. This article is an open access article distributed under the terms and conditions of the Creative Commons Attribution (CC BY) license (https://creativecommons.org/licenses/by/4.0/).

1. Introduction

Multiple advantages of the controller area network (CAN), such as good real-time performance, reliability, and scalability at low cost, make it widely applied in in-vehicle communication systems, industrial automation control, aviation communication systems, and other fields with strict reliability requirements [1]. However, in practice, various adverse factors such as improper human intervention, ambient interference, vibration and wear of electronic equipment, and aging-related degradation can lead to intermittent faults that deteriorate network reliability. An intermittent connection (IC) fault is a randomly occurring and shortly persistent wiring problem, usually resulting from cable fatigue, insulation wear, vibration, and aging loosening in harsh working conditions. The IC fault is a hidden problem and a potential threat to system reliability. In the early stages, IC faults may interrupt normal message transmission, leading to delays or loss of messages, which worsens network service quality and degrades system performance. In severe cases, the IC fault-induced communication errors can cause a node to enter the bus-off state, which may cause system-level failures in the safety-critical systems, increase the maintenance cost of the networks, and even lead to security incidents [2]. Therefore, there is an urgent need for CAN to detect and locate IC faults before they cause system-wide damage.

In the literature, the fault diagnosis of CAN has been studied in various aspects. Kelkar and Kamal [3] developed an adaptive fault diagnosis algorithm to detect faulty CAN nodes. Yang et al. [4] detected persistent anomalies in CAN buses, such as terminal resistance loss

and cable degradation. Wang et al. [5] applied a resistance detection method to detect and locate the CAN bus permanent fault. However, the methods in [3–5] can only diagnose fault nodes or permanent faults, which are not applicable to intermittent faults.

In recent years, there has been extensive research on intermittent faults in electrical systems. Fang et al. [6] proposed an intermittent fault recognition method for analog circuits based on density peak clustering. Gouda et al. [7] proposed a one-shot likelihood ratio test method for evaluating the intermittent fault status of a sensor node in wireless sensor networks. Zhang et al. [8] proposed a residual evaluation model to detect sensor intermittent faults. However, the practical procedure for locating intermittent faults is not addressed by [6–8].

Subsequently, studies were also conducted to locate intermittent faults in several electrical systems. Huang et al. [9] proposed a deep forest classifier for analog circuits to localize intermittent faults. Yu et al. [10] developed a composite degradation model-based intermittent fault detection and isolation method for a steer-by-wire system. Farughian et al. [11] proposed an intermittent earth fault passage diagnosis method for a compensated distribution network to locate faulty segments. However, these methods are constrained to specific devices or ad hoc systems and cannot handle the intermittent faults in CAN.

Recently, various aspects of intermittent faults in CAN have been studied. In [12,13], the network performance analysis methods under intermittent faults, such as electrical fast transient (EFT) and electromagnetic interference (EMI) were developed. However, the localization technique for the intermittent fault of cable connection types still needs to be developed. Subsequently, some preliminary research focused on the intermittent open circuit (IOC) fault diagnosis for CANs. For example, Zhang et al. [14] proposed a context-free-grammar-based IOC fault diagnosis method using data-link layer information. Zhang et al. [15] proposed a tree-based unified IOC fault diagnostic framework. Wang et al. [16] proposed a fault symptom association model-based method to diagnose various IOC fault location scenarios. However, these methods are limited to simple bus topologies and unsuitable for complex ones such as tree topologies. Wang et al. [17] proposed an IOC fault diagnosis method for complex topological CANs using a divide-and-conquer strategy. However, the diagnosis methods in [14–17] can only deal with open circuit faults but not short circuit faults.

Additionally, the researchers also studied short circuit faults in various electrical systems. Li et al. [18] proposed a deep learning-based method for short-circuit fault diagnosis in the transmission line. Using the power distribution information, Gao et al. [19] developed an Elman neural network-based short circuit fault section location method for the 10 kV distribution network. Nevertheless, they are designed specifically for three-phase power systems and are not suitable for CAN. Bani Milhim et al. [20] proposed a voltage measurement-based method to identify the CAN physical fault types, including open electrical connections and shorted wires. However, the technique of locating the shorted wire is not addressed. Krishnamurthy et al. [21] localized the open and short wire faults on the CAN bus using a time-domain reflectometry (TDR) method. However, the TDR-based method does not apply to intermittent faults [22,23]. In addition, this reflectometry method may lead to the wrong localization results due to reflections of the injected signal at junctions of network branches or at device connections [23], and the method requires arranging additional transmitters and receivers in the system, which limits the applicability of the method [24]. Du et al. [25] developed a current measurement-based short-fault distance mapping approach for the CAN bus. However, this method also does not apply to situations where short circuits occur intermittently, i.e., intermittent short circuit (ISC) faults. Moreover, this simple series circuit model cannot reasonably describe and diagnose the complex topologies with multiple branches. Furthermore, this method requires a shunt resistor to be embedded inside a node to measure the current, which is practically inconvenient to implement and its location accuracy relies on the measurement precision of the tiny shunt resistor, which is not robust and prone to incorrect mapping results.

Table 1 summarizes the main aspects and gaps in the existing literature. As can be seen from Table 1, existing CAN intermittent fault diagnosis methods have addressed EMI, EFT, and cable open faults but not cable short faults, whereas existing CAN short circuit fault diagnosis methods have addressed permanent short circuit faults but not common intermittent short circuit (ISC) faults. Even the existing short fault diagnosis methods for CANs [20,21,25] still have the following drawbacks. First, the data acquisition (DAQ) system needs to be embedded inside the node, which is not always practical in real applications. Second, these methods are limited to the simple bus topology layout but cannot be used for complex multi-branch topology layouts because the junctions of network branches are not modeled. Third, these methods cannot solve the short circuit faults with intermittent property, i.e., ISC faults. The ISC fault is a hard troubleshooting problem for existing offline methods [17]. First, ISC faults are typically caused by cable fatigue and deteriorated electric insulation in vibrating environments; these conditions cannot be repeated during system shutdowns. Second, since CAN nodes share the bus media and cable short circuits can impact the bus system-wide, the fault location usually has no explicit mapping to the bus-off node. Therefore, it is essential to develop a systematic ISC fault diagnosis method that is effective in various CAN topologies and easy to implement without interrupting normal system operations, as indicated by the gap covered by this work highlighted in Table 1.

Table 1. Summary of related work.

Ref.	Main Approach	Research Gap
[3–5]	Permanent fault diagnosis for CANs	Diagnostics for the intermittent faults
[6–8]	Intermittent fault detection for electrical systems	Localization techniques for intermittent faults
[9–11]	Intermittent fault localization for specific systems	Relevant technique used for CANs
[12,13]	Performance analysis of CANs with intermittent faults such as EMI/EFT	Localization techniques for intermittent faults in cable connection types
[14–16]	Intermittent open circuit fault diagnosis for the bus topology CANs	Diagnostics for short circuit faults and for complex network topologies
[17]	Intermittent open circuit fault diagnosis for the tree topology CANs	Diagnostics for short circuit faults
[18,19]	Short circuit diagnosis for three-phase power systems	Relevant technique used for CANs
[20]	Recognition of short and open circuit faults in CANs	Localization techniques for short circuit faults
[21]	Localization of permanent short and open wire faults in CANs based on TDR	Diagnostics for faults with intermittent nature and for complex network topologies
[25]	Distance mapping of short circuit faults in CANs based on the current measurement	Diagnostics for intermittent faults and for complex topologies/Practicality of DAQ scheme
This work	Localization of intermittent short circuit (ISC) faults in CANs supported by the two-port network modeling	(Covered gap) Correctly locate ISC faults in various topologies with easy implementation

This paper proposes a novel ISC fault location method based on two-port networks without interrupting normal system operation. The contributions of this work are as follows:

- Using two-port network techniques to model the equivalent circuits of the CAN switched system that depends on sending states of distinct nodes, *a generic diagnostic framework for multiple network topologies* is developed, especially complex topologies that existing methods cannot handle.
- Based on voltage transfer difference function groups for CAN switched subsystems that are separately preset with two types of fault locations, *a bidirectional eviction location strategy to identify various ISC fault location scenarios* is proposed, including single-fault and multi-fault scenarios.

- This method only needs to collect voltages at the network port to localize ISC faults, *with no need to consider accessibility inside the network*.

The results of this work will promote a comprehensive diagnosis of various intermittent connection faults in CANs, which should lead to more targeted maintenance actions for CAN-based systems and ensure system reliability.

The rest of this paper is organized as follows: Section 2 introduces the CAN fault handling mechanism and defines the problems faced in this work. In Section 3, the ISC fault localization method is developed, including two-port network modeling, voltage transfer difference function groups, and the bidirectional eviction localization approach. In Section 4, the case studies to demonstrate the effectiveness of the proposed method are conducted. In Section 5, the robustness and limitations of the proposed method are discussed. Conclusions and future work are presented in Section 6.

2. Preliminaries

2.1. CAN Fault Handling Mechanism

CAN bus is a two-wire bus using a DC-coupled differential signal system with two logical states, recessive and dominant [15,26]. The dominant state is when the differential voltage is above 0.9 V, and the recessive state is when the differential voltage is below 0.5 V [27]. According to the CAN specification [28], the standard CAN data frame contains seven fields, as shown in Figure 1, where the arbitration field contains the 11-bit identifier that provides the priority and source address of the frame.

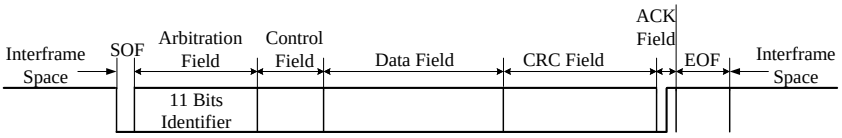


Figure 1. Schematic of standard CAN data frame.

Five types of error can be detected, which are bit error, stuff error, CRC error, form error, and acknowledgment error. Any error-active node that detects an error condition will send an error-active flag to interrupt the current data frame transmission. The error-active flag consists of six consecutive dominant bits. The communication will resume when the bus is idle again [26].

2.2. Problem Definition and Assumptions

The ISC fault will cause a short-time connection between CAN-H and CAN-L, and the resulting short circuit will turn the dominant bit into the recessive bit due to significantly pulling down the differential voltage to less than 0.9V. Because the short circuit globally acts on the entire CAN bus, the data link layer behavior anywhere on the network during the ISC fault is uniformly dominant to recessive. Thus, locating ISC faults based on data link layer information, such as error flags and corrupted data frames is challenging. Therefore, we consider extracting the fault features from the physical layer for ISC fault localization. Based on this consideration, the following issues should be addressed:

(1) How can a suitable model for the CAN bus containing ISC faults be established so that the internal network voltage can be derived from information collected at easily measurable network terminals?
(2) How can the physical layer fault features, e.g., the bus voltage, be captured and extracted at the ISC occurrence moment?
(3) How can all ISC faults in the network be systematically located based on the bus model and physical layer fault feature?

The assumptions of this work are as follows: (1) The CAN signal is always in the circuit-steady state due to the energy absorption effect of the terminal resistor; thus, dynamic components like capacitors and inductors are not considered. (2) Without loss of generality, we assume that all nodes in the network are in the error-active state. (3) The ISC faults are

independent and persistent over time, and the chance that two or more ISC faults occur in one data frame is negligibly low. (4) To simplify the equations and calculations, we assume that the cables between every two nodes are equal in length and resistance.

3. Methodology

In this paper, an ISC fault diagnosis method for CAN is proposed based on the two-port network modeling. The basic idea of this work is that by considering CAN as a switched system that switches among different sending node states and using a two-port modeling technique to describe the switched subsystems that are preset separately with two possible types of ISC locations, the voltage of the sending node can be calculated, respectively, from the voltage at each network end via the voltage transfer functions, where the voltage transfer function using the correct ISC location minimizes the difference between that two calculated sending node voltages.

The framework of the method is shown in Figure 2. First, the equivalent circuits of the CAN bus-switched system with sending states of distinct nodes are modeled using two-port networks. For each switched subsystem, a voltage transfer difference function group (VTDFG) is derived based on two assumptions: an ISC fault is separately on individual sides of the sending node. Once an ISC fault occurs, the data acquisition (DAQ) phase first identifies the sending node of the corrupted frame to determine the VTDFG to be used and then extracts the voltages of all network ends at the ISC occurrence moment, i.e., the fault voltages. The corresponding direction events are defined by evaluating the two VTDFG values calculated from the fault voltages. Then, these direction events are combined with topology information to derive fault or health domains based on their statistical significance. Finally, a bidirectional eviction localization (BEL) approach is developed to identify ISC fault locations in the network using the fault and health domains of all nodes. The details of the proposed method are introduced as follows:

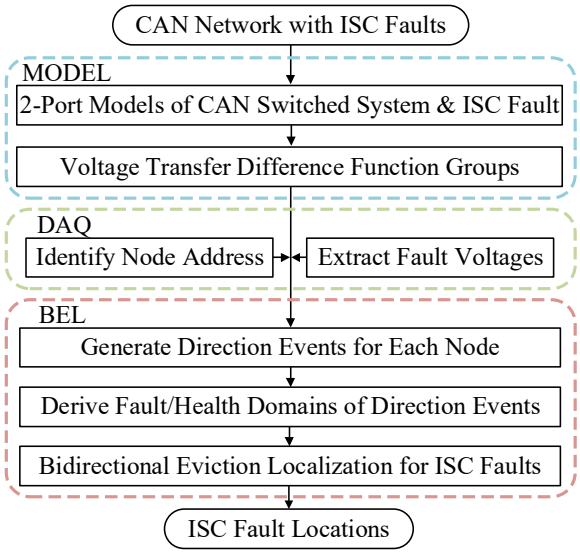


Figure 2. Framework of ISC fault diagnosis method.

3.1. System Modeling by Two-Port Networks

Figure 3 shows the equivalent circuit model (ECM) of the CAN bus with ISC faults, where three branches X, Y, and Z are, respectively, connected to x, y, and z nodes, node X_1 refers the first node on branch X and is denoted as N_{X_1}, R_{T_X} and R_{T_Y} denote the terminal resistors, $R_{m,m\in\{1,2,\ldots,\circ\},\circ\in\{x,y,z\}}$ denotes the differential internal resistor of node $\bullet_{m,\bullet\in\{X,Y,Z\}}$, r denotes the cable resistor of the link between nodes, R_S denotes the short-circuit contact resistor, and the power source $E_{k,k\in\{1,2,\ldots,\circ\},\circ\in\{x,y,z\}}$ represents the CAN-switched subsystem with the sending node $\bullet_{k,\bullet\in\{X,Y,Z\}}$. Note that the CAN signal is assumed to be in the circuit steady state, so dynamic components such as capacitors

and inductors are not considered in this work. As shown in Figure 3, the ECM can be decomposed into the sending node, the receiving node, the faulty node, the coupling unit, and the terminal resistor. Details of these components are introduced as follows:

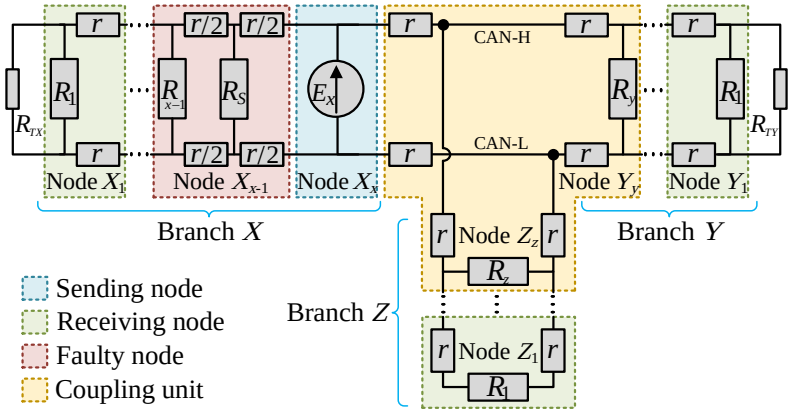


Figure 3. ECM of the tree-topological CAN with an ISC fault.

3.1.1. Receiving Node

The receiving node refers to the node receiving messages, which consists of a node differential internal resistor and two cable resistors. Figure 4a shows the two-port model of the receiving node $\bullet_{i,\bullet\in\{X,Y,Z\}}$, whose transmission parameter equation is

$$\begin{bmatrix} U_{i+1} \\ I_i \end{bmatrix} = \underbrace{\begin{bmatrix} 1+\frac{2r}{R_i} & 2r \\ \frac{1}{R_i} & 1 \end{bmatrix}}_{\mathbf{A}_i} \begin{bmatrix} U_i \\ I_{i-1} \end{bmatrix} \tag{1}$$

Moreover, it can be obtained from (1) that

$$U_{i+1} = \underbrace{\begin{bmatrix} 1+\frac{2r}{R_i} & 2r \end{bmatrix}}_{\mathbf{B}_i} \begin{bmatrix} U_i \\ I_{i-1} \end{bmatrix} \tag{2}$$

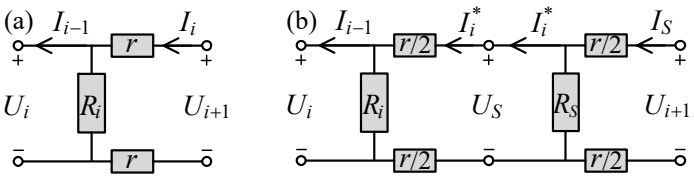


Figure 4. Two-port modeling of (**a**) a receiving node and (**b**) a faulty node.

3.1.2. Faulty Node

The faulty node is defined as a receiving node with a short-circuit contact resistor connected to the middle of the cable resistors. In this work, only the case where the faulty node is next to the sending node needs to be considered. Figure 4b shows the two-port model of a faulty node, whose transmission parameter equation can be obtained based on (1) and (2), i.e.,

$$U_{i+1} = \underbrace{\overbrace{\begin{bmatrix} 1+\frac{r}{R_S} & r \end{bmatrix}}^{\mathbf{B}^S} \begin{bmatrix} 1+\frac{r}{R_i} & r \\ \frac{1}{R_i} & 1 \end{bmatrix}}_{\mathbf{B}_i^S} \begin{bmatrix} U_i \\ I_{i-1} \end{bmatrix} \tag{3}$$

3.1.3. Coupling Unit

The coupling unit represents the intersection of branches [17]. Figure 5a shows the two-port model of a coupling unit, whose transmission parameter equation is

$$\begin{bmatrix} U_x \\ I_x \end{bmatrix} = \underbrace{\begin{bmatrix} \frac{1}{2}+\frac{3r}{R_y} & 3r \\ \frac{1}{R_y} & 1 \end{bmatrix}}_{\mathbf{O}_y} \begin{bmatrix} U_y \\ I_y \end{bmatrix} + \underbrace{\begin{bmatrix} \frac{1}{2}+\frac{3r}{R_z} & 3r \\ \frac{1}{R_z} & 1 \end{bmatrix}}_{\mathbf{O}_z} \begin{bmatrix} U_z \\ I_z \end{bmatrix} \tag{4}$$

Moreover, it can be obtained from (4) that

$$U_x = \underbrace{\begin{bmatrix} \frac{1}{2}+\frac{3r}{R_y} & 3r \end{bmatrix}}_{\mathbf{Q}_y} \begin{bmatrix} U_y \\ I_y \end{bmatrix} + \underbrace{\begin{bmatrix} \frac{1}{2}+\frac{3r}{R_z} & 3r \end{bmatrix}}_{\mathbf{Q}_z} \begin{bmatrix} U_z \\ I_z \end{bmatrix} \tag{5}$$

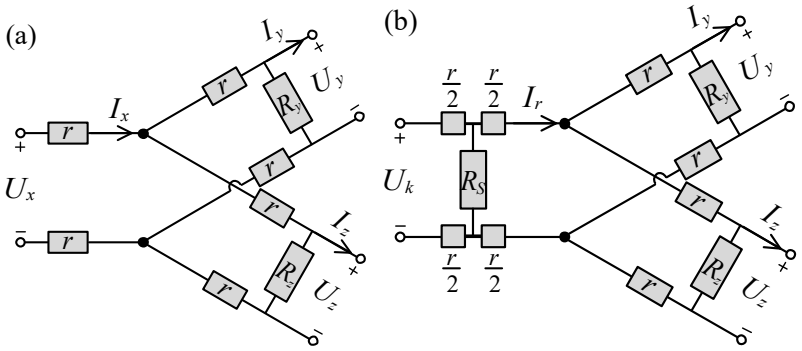


Figure 5. Two-port modeling of coupling units (**a**) for normal condition and (**b**) with an ISC fault.

Especially, when the coupling unit contains the ISC fault, as shown in Figure 5b, the transmission parameter equation is (6), where $\mathbf{B}^S$ is defined in (3).

$$U_k = \mathbf{B}^S \left(\underbrace{\begin{bmatrix} \frac{1}{2}+\frac{2r}{R_y} & 2r \\ \frac{1}{R_y} & 1 \end{bmatrix}}_{\mathbf{V}_y} \begin{bmatrix} U_y \\ I_y \end{bmatrix} + \underbrace{\begin{bmatrix} \frac{1}{2}+\frac{2r}{R_z} & 2r \\ \frac{1}{R_z} & 1 \end{bmatrix}}_{\mathbf{V}_z} \begin{bmatrix} U_z \\ I_z \end{bmatrix} \right) \tag{6}$$

By cascading the two-port models of receiving nodes, faulty nodes, and coupling units, the voltage relationship between the end of the network and the sending node can be built, based on which the following function group is designed.

3.2. Voltage Transfer Difference Function Group (VTDFG)

For further analysis, the main terminal of a node is defined as the end of the branch where this node is located, while the ends of other branches are the sub-terminals of this node. For example, in Figure 3, the main terminal of N_{Y_1} is T_Y, and the sub-terminals of N_{Z_1} are T_X and T_Y.

For the switched subsystem with the sending node $\bullet_{k,\bullet\in\{X,Y,Z\}}$, its VTDFG is defined as the two possible differences between the two voltages of $N_{\bullet_k}$, calculated from the voltages of the main-terminal and sub-terminals, respectively, under the two possible cases where the ISC fault is on the main-terminal side and sub-terminal side of $N_{\bullet_k}$.

Depending on whether the branch where the sending node is located contains the terminal resistor, the VTDFG is categorized into two cases. First, for the branch with a terminal resistor, such as branch X, the VTDFG of node $N_{X_{k,k\in\{2,3,\ldots,x\}}}$ is shown in (7), where $VTDF^{N_{X_k}}_{T_h,h\in\{main,sub\}}$ denotes the VTDF assuming that the fault is on the T_h-side of node N_{X_k}, $\mathbf{P}_{T_{u,u\in\{X,Y\}}} = \begin{bmatrix} U_{T_u} & \frac{U_{T_u}}{R_{T_u}} \end{bmatrix}^{\mathrm{T}}$, $\mathbf{P}_{T_Z} = \begin{bmatrix} \frac{R_1+2r}{R_1} U_{T_Z} & \frac{U_{T_Z}}{R_1} \end{bmatrix}^{\mathrm{T}}$, and $\mathbf{A}_i, \mathbf{B}_i, \mathbf{B}^S, \mathbf{B}^S_i, \mathbf{O}_i, \mathbf{Q}_i, \mathbf{V}_i$ are defined in (1)–(6). Since the symmetry of the network and the VTDFG of the node on branch Y can be obtained by exchanging "X" and "Y" in (7). Second, for the branch without a terminal resistor, such as branch Z, the VTDFG of node $N_{Z_{k,k\in\{2,3,\ldots,z\}}}$ is shown in (8).

$$\begin{cases} VTDF_{T_{main}}^{N_{X_k}} = \begin{cases} \left| \mathbf{B}_{k-1}^{S} \prod_{i=k-2}^{1} \mathbf{A}_i \mathbf{P}_{T_X} - \mathbf{B}_{k+1} \prod_{j=k+2}^{x} \mathbf{A}_j \left(\mathbf{O}_y \prod_{p=y-1}^{1} \mathbf{A}_p \mathbf{P}_{T_Y} + \mathbf{O}_z \prod_{q=z-1}^{2} \mathbf{A}_q \mathbf{P}_{T_Z} \right) \right|, & k \in \{2,3,\ldots,x-1\} \\ \left| \mathbf{B}_{x-1}^{S} \prod_{i=x-2}^{1} \mathbf{A}_i \mathbf{P}_{T_X} - \left(\mathbf{Q}_y \prod_{p=y-1}^{1} \mathbf{A}_p \mathbf{P}_{T_Y} + \mathbf{Q}_z \prod_{q=z-1}^{2} \mathbf{A}_q \mathbf{P}_{T_Z} \right) \right|, & k = x \end{cases} \\ VTDF_{T_{sub}}^{N_{X_k}} = \begin{cases} \left| \mathbf{B}_{k-1} \prod_{i=k-2}^{1} \mathbf{A}_i \mathbf{P}_{T_X} - \mathbf{B}_{k+1}^{S} \prod_{j=k+2}^{x} \mathbf{A}_j \left(\mathbf{O}_y \prod_{p=y-1}^{1} \mathbf{A}_p \mathbf{P}_{T_Y} + \mathbf{O}_z \prod_{q=z-1}^{2} \mathbf{A}_q \mathbf{P}_{T_Z} \right) \right|, & k \in \{2,3,\ldots,x-1\} \\ \left| \mathbf{B}_{x-1} \prod_{i=x-2}^{1} \mathbf{A}_i \mathbf{P}_{T_X} - \mathbf{B}^{S} \left(\mathbf{V}_y \prod_{p=y-1}^{1} \mathbf{A}_p \mathbf{P}_{T_Y} + \mathbf{V}_z \prod_{q=z-1}^{2} \mathbf{A}_q \mathbf{P}_{T_Z} \right) \right|, & k = x \end{cases} \end{cases} \tag{7}$$

$$\begin{cases} VTDF_{T_{main}}^{N_{Z_k}} = \begin{cases} \left| \mathbf{B}^{S} \mathbf{P}_{T_Z} - \mathbf{B}_3 \prod_{j=4}^{z} \mathbf{A}_j \left(\mathbf{O}_x \prod_{p=x-1}^{1} \mathbf{A}_p \mathbf{P}_{T_X} + \mathbf{O}_y \prod_{q=y-1}^{1} \mathbf{A}_q \mathbf{P}_{T_Y} \right) \right|, & k = 2 \\ \left| \mathbf{B}_{k-1}^{S} \prod_{i=k-2}^{2} \mathbf{A}_i \mathbf{P}_{T_Z} - \mathbf{B}_{k+1} \prod_{j=k+2}^{z} \mathbf{A}_j \left(\mathbf{O}_x \prod_{p=x-1}^{1} \mathbf{A}_p \mathbf{P}_{T_X} + \mathbf{O}_y \prod_{q=y-1}^{1} \mathbf{A}_q \mathbf{P}_{T_Y} \right) \right|, & k \in \{3,4,\ldots,z-1\} \\ \left| \mathbf{B}_{z-1}^{S} \prod_{i=z-2}^{2} \mathbf{A}_i \mathbf{P}_{T_Z} - \left(\mathbf{Q}_x \prod_{p=x-1}^{1} \mathbf{A}_p \mathbf{P}_{T_X} + \mathbf{Q}_y \prod_{q=y-1}^{1} \mathbf{A}_q \mathbf{P}_{T_Y} \right) \right|, & k = z \end{cases} \\ VTDF_{T_{sub}}^{N_{Z_k}} = \begin{cases} \left| \frac{R_1 + 2r}{R_1} U_{T_Z} - \mathbf{B}_3^{S} \prod_{j=4}^{z} \mathbf{A}_j \left(\mathbf{O}_x \prod_{p=x-1}^{1} \mathbf{A}_p \mathbf{P}_{T_X} + \mathbf{O}_y \prod_{q=y-1}^{1} \mathbf{A}_q \mathbf{P}_{T_Y} \right) \right|, & k = 2 \\ \left| \mathbf{B}_{k-1} \prod_{i=k-2}^{2} \mathbf{A}_i \mathbf{P}_{T_Z} - \mathbf{B}_{k+1}^{S} \prod_{j=k+2}^{z} \mathbf{A}_j \left(\mathbf{O}_x \prod_{p=x-1}^{1} \mathbf{A}_p \mathbf{P}_{T_X} + \mathbf{O}_y \prod_{q=y-1}^{1} \mathbf{A}_q \mathbf{P}_{T_Y} \right) \right|, & k \in \{3,4,\ldots,z-1\} \\ \left| \mathbf{B}_{z-1} \prod_{i=z-2}^{2} \mathbf{A}_i \mathbf{P}_{T_Z} - \mathbf{B}^{S} \left(\mathbf{V}_x \prod_{p=x-1}^{1} \mathbf{A}_p \mathbf{P}_{T_X} + \mathbf{V}_y \prod_{q=y-1}^{1} \mathbf{A}_q \mathbf{P}_{T_Y} \right) \right|, & k = z \end{cases} \end{cases} \tag{8}$$

3.3. Data Acquisition and Analysis

To capture the unknown information in the VTDFG, i.e., the sending node address $\bullet_{k,\bullet \in \{X,Y,Z\}}$ and the network terminal voltages U_{T_X}, U_{T_Y}, and U_{T_Z} at the fault occurrence moment, the field programmable gate array (FPGA)-based data acquisition (DAQ) sensor is deployed at the terminal of each branch to record error messages. Once an error flag containing consecutive six dominant bits appears on the bus, the DAQ sensor is triggered to record the error message. For example, a recorded error message is shown in Figure 6.

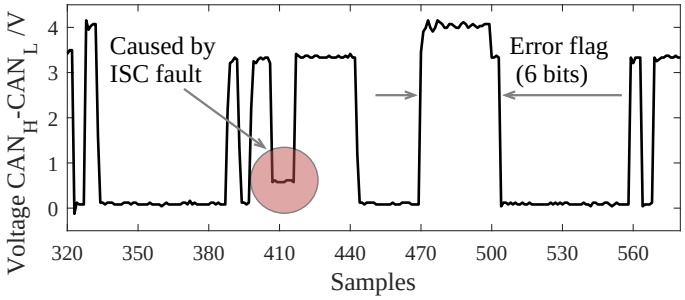


Figure 6. Example of CAN analog waveform when an ISC fault occurs.

As shown in Figure 6, the bus differential voltage during the ISC fault is much lower than the normal dominant voltage, which cannot be recognized as a dominant bit since it is less than 0.9 V [27]. Therefore, once the bus differential voltage enters the range of 0 to 0.9 V, it is extracted as the fault voltage. Meanwhile, the sending node address of the error message can be obtained by directly reading the arbitration field of the data frame.

3.4. Definition of Direction Events

As soon as the sending node address and fault voltages of an error message are determined, the VTDFG can be solved, and then the comparison between the two VTDFG values can be conducted.

If $VTDF_{T_{main}}^{N_{\bullet_k}} < VTDF_{T_{sub},\bullet\in\{X,Y,Z\}}^{N_{\bullet_k}}$, it indicates that there are ISC faults occurring on the links between the node $N_{\bullet_k}$ and the terminal T_{main}. Then the direction event $\mathcal{E}_{T_{main}}^{N_{\bullet_k}}$ is produced. While if $VTDF_{T_{main}}^{N_{\bullet_k}} > VTDF_{T_{sub},\bullet\in\{X,Y,Z\}}^{N_{\bullet_k}}$, it indicates that there are ISC faults occurring on the links between the node $N_{\bullet_k}$ and the terminal T_{sub}. Then the direction event $\mathcal{E}_{T_{sub}}^{N_{\bullet_k}}$ is produced.

Therefore, each direction event of a node contains rough location information about where between the terminal and node the ISC fault occurs. Then, the ISC fault can be precisely located to a specific link by combining the direction events of all nodes with the network topology, as detailed in the following sections.

3.5. Domain of Direction Events

For further analysis, let $\mathcal{P}_{N_{\bullet_k}-T_h,\bullet\in\{X,Y,Z\},h\in\{main,sub\}}$ denote the communication path between node $N_{\bullet_k}$ and terminal T_h, and $\mathcal{L}_{N_{\bullet_k}-T_h}$ denote the set of all links that form $\mathcal{P}_{N_{\bullet_k}-T_h}$.

Definition 1. *Fault Domain—the fault domain of the direction event $\mathcal{E}_{T_h}^{N_{\bullet_k}}$ is a set of suspected faulty links derived from this direction event, which is denoted as $\mathcal{FT}_{T_h}^{N_{\bullet_k}}$.*

Each node will have a sufficient number of direction events as ISC faults persist over time. In this paper, only the direction events whose ratios are more than 1% are considered significant. Based on the definition of direction events, if the direction event $\mathcal{E}_{T_h}^{N_{\bullet_k}}$ is significant, then there are ISC faults occurring on $\mathcal{P}_{N_{\bullet_k}-T_h}$, and any link in $\mathcal{L}_{N_{\bullet_k}-T_h}$ is suspected to suffer ISC faults. Hence, the fault domain of $\mathcal{E}_{T_h}^{N_{\bullet_k}}$, i.e., $\mathcal{FT}_{T_h}^{N_{\bullet_k}}$, derived by

$$\mathcal{FT}_{T_h}^{N_{\bullet_k}} = \{l_c | l_c \in \mathcal{L}_{N_{\bullet_k}-T_h}\}, \text{s.t.}, \mathcal{E}_{T_h}^{N_{\bullet_k}} \text{ is statistically significant} \tag{9}$$

Definition 2. *Health Domain—the health domain of the direction event $\mathcal{E}_{T_h}^{N_{\bullet_k}}$ is a set of healthy links derived from this direction event, which is denoted as $\mathcal{HL}_{T_h}^{N_{\bullet_k}}$.*

If the direction event $\mathcal{E}_{T_h}^{N_{\bullet_k}}$ is not significant, then there is no ISC fault occurring on $\mathcal{P}_{N_{\bullet_k}-T_h}$, and every link in $\mathcal{L}_{N_{\bullet_k}-T_h}$ is free of ISC faults. Hence, the health domain of $\mathcal{E}_{T_h}^{N_{\bullet_k}}$, i.e., $\mathcal{HL}_{T_h}^{N_{\bullet_k}}$, derived by

$$\mathcal{HL}_{T_h}^{N_{\bullet_k}} = \{l_c | l_c \in \mathcal{L}_{N_{\bullet_k}-T_h}\}, \text{s.t.}, \mathcal{E}_{T_h}^{N_{\bullet_k}} \text{ is not statistically significant} \tag{10}$$

3.6. Bidirectional Eviction Localization (BEL) of ISC Faults

ISC fault localization can be converted to a process of finding such a set of locations that can result in all fault domains of all nodes while not leading to any health domains. Hence, the domains produced by the two terminals need to be analyzed separately. The T_h-direction localization uses all the domains from the terminal $T_{h,h\in\{main,sub\}}$, i.e.,

$$ISC_{T_h} = \bigcap_{\bullet=X}^{Z} \bigcap_{k=1}^{\circ} \mathcal{FT}_{T_h}^{N_{\bullet_k}} - \bigcup_{\bullet=X}^{Z} \bigcup_{k=1}^{\circ} \mathcal{HL}_{T_h}^{N_{\bullet_k}} \tag{11}$$

where $ISC_{T_h,h\in\{main,sub\}}$ denotes the T_h-direction localization result and $\circ \in \{x, y, z\}$ is the number of nodes in corresponding branch $\bullet \in \{X, Y, Z\}$.

The complete ISC fault location in the network is the concatenation of T_{main}-direction and T_{sub}-direction localization results. Therefore, the set of ISC fault locations in the network, $ISC_{Network}$, can be derived by

$$ISC_{Network} = ISC_{T_{main}} \bigcup ISC_{T_{sub}} \tag{12}$$

4. Experiments

A testbed is constructed, and three case studies are conducted to demonstrate the effectiveness of the proposed method. In case study 1, a single-fault scenario on the simple bus topology is used to detail the analysis procedure. In case study 2, a multiple-fault scenario is used to verify the differentiation capability for ISC fault locations of the method. In case study 3, the scenario of ISC faults on the tree topology is studied to demonstrate the topology universality of the method.

4.1. Testbed Setup

The constructed testbed is shown in Figure 7, which consists of a CAN communication module, an ISC fault injection module, and a DAQ module. The CAN communication module is constructed by DeviceNet hardware, which uses the CAN protocol as the bottom communication protocol. The communication mode is polling, the cycle time is 10 ms, and the communication rate is 500 Kbps. The ISC faults are emulated by controlling the high-speed on-off of the ADG801 normally open switch, where the switch connects CAN-H and CAN-L. The PC program independently controls the ISC faults on different cables via different switches, the arrival of faults follows the Poisson process, and the duration of each fault is set to be 2-bit length, i.e., 4 µs. The DAQ module is developed on an FPGA-based DAQ framework on NI CRIO hardware, and each acquisition is triggered by detecting consecutive 6 dominant bits.

The resistance values of the components in the system are as follows: The cable resistance $r \approx 0.5\ \Omega$, can be obtained from the standard resistivity parameter of the cable or by direct measurement. According to ISO 11898-2 [27], the terminal resistance $R_{T_h} = 120\ \Omega$, the differential internal resistance of the node receiver $R_m \in [12, 100]$ kΩ, and the median $R_m = 56$ kΩ is used in this work (note that the node resistance R_m is much larger than the other parameters and it acts as a denominator in the VTDFG, so its value in the specified interval has almost no effect on the localization result, which is discussed in Section 5). The short-circuit contact resistance is the on-resistance of the ADG801 switch, i.e., $R_S = 0.25\ \Omega$.

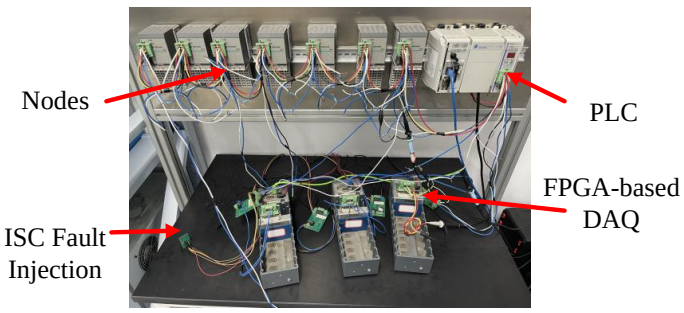


Figure 7. The constructed testbed for case studies.

4.2. Case Study 1: Single ISC Fault on Simple Topology

4.2.1. Method Simplification

To facilitate the reader's understanding, the scenario that the ISC fault on the simple bus topology is studied, as shown in Figure 8.

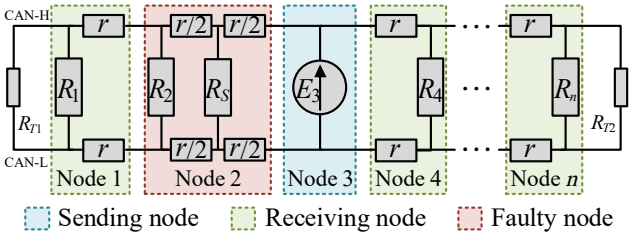


Figure 8. ECM of the bus-topological CAN with an ISC fault.

First, the ECM of the bus-topological CAN only includes sending nodes, faulty nodes, and receiving nodes. Hence, the VTDFG of the sending node $N_{k,k\in\{1,2,\ldots,n\}}$ can be simplified to (13), where $\mathbf{P}_{T_{h,h\in\{1,2\}}} = \left[U_{T_h} \quad \frac{U_{T_h}}{R_{T_h}}\right]^{\mathrm{T}}$. Second, the DAQ process is the same as in Section 3.3, but the sensors only need to be deployed at both ends of the network. Finally, the definition and the domain of direction events, and the BEL process are the same as in Section 3.4, Section 3.5 and Section 3.6, respectively, except replacing T_{main} with T_1, T_{sub} with T_2, and (11) with (14).

$$\begin{cases} VTDF_{T_1}^{N_k} = \left| \mathbf{B}_{k-1}^{S} \prod_{i=k-2}^{1} \mathbf{A}_i \mathbf{P}_{T_1} - \mathbf{B}_{k+1} \prod_{j=k+2}^{n} \mathbf{A}_j \mathbf{P}_{T_2} \right| \\ VTDF_{T_2}^{N_k} = \left| \mathbf{B}_{k-1} \prod_{i=k-2}^{1} \mathbf{A}_i \mathbf{P}_{T_1} - \mathbf{B}_{k+1}^{S} \prod_{j=k+2}^{n} \mathbf{A}_j \mathbf{P}_{T_2} \right| \end{cases} \tag{13}$$

$$ISC_{T_h} = \bigcap_{k=1}^{n} \mathcal{FT}_{T_h}^{N_k} - \bigcup_{k=1}^{n} \mathcal{HL}_{T_h}^{N_k} \tag{14}$$

4.2.2. Experiment Verification

In this case study, as case A shown in Figure 9, the ISC faults occur on the link between nodes 1 and 2, i.e., l_1. In total, 1705 error messages are recorded in this case study.

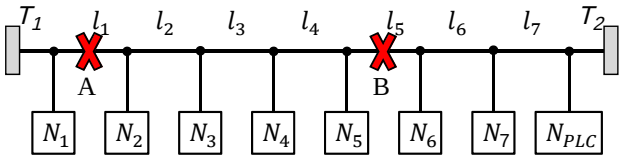


Figure 9. Network topology and fault setups in case studies 1 and 2. The red crosses denote the ISC faults. A and B denote the cases where the faults occur on links l_1 and l_5, respectively.

Step 1. Produce Direction Events: Based on the VTDFG for bus topology (13), the types of direction events, as well as the ratio of each type over a total number of records for all nodes can be obtained, as shown in Table 2.

Step 2. Derive Domains: The fault domains and health domains for all nodes can be derived by (9) and (10), respectively, as shown in Table 3.

Step 3. Locate ISC Faults: By using the domains for all nodes obtained from sensor T_1 and (14), the T_1-direction location result is $ISC_{T_1} = \{l_1\} - \varnothing = \{l_1\}$. By using the domains for all nodes obtained from sensor T_2 and (14), the T_2-direction location result is $ISC_{T_2} = \{l_1, l_2, l_3, l_4, l_5, l_6, l_7\} - \{l_2, l_3, l_4, l_5, l_6, l_7\} = \{l_1\}$. Therefore, the set of ISC fault locations is $ISC_{Network} = ISC_{T_1} \bigcup ISC_{T_2} = \{l_1\}$, which agrees with the experimental setup.

Table 2. Direction events and corresponding ratio for nodes in case study 1.

N_k	N_1	N_2	N_3	N_4	N_5	N_6	N_7	N_{PLC}
$\mathcal{E}_{T_1}^{N_k}$	0	99.4%	99.4%	100%	100%	100%	99.3%	100%
$\mathcal{E}_{T_2}^{N_k}$	100%	0.6%	0.6%	0	0	0	0.7%	0

Table 3. Fault domains and health domains of direction events in case study 1.

N_k	$\mathcal{FT}_{T_1}^{N_k}$	$\mathcal{HL}_{T_1}^{N_k}$	$\mathcal{FT}_{T_2}^{N_k}$	$\mathcal{HL}_{T_2}^{N_k}$
N_1	–	$\varnothing$	$\{l_1, l_2, l_3, l_4, l_5, l_6, l_7\}$	–
N_2	$\{l_1\}$	–	–	$\{l_2, l_3, l_4, l_5, l_6, l_7\}$
N_3	$\{l_1, l_2\}$	–	–	$\{l_3, l_4, l_5, l_6, l_7\}$
N_4	$\{l_1, l_2, l_3\}$	–	–	$\{l_4, l_5, l_6, l_7\}$
N_5	$\{l_1, l_2, l_3, l_4\}$	–	–	$\{l_5, l_6, l_7\}$
N_6	$\{l_1, l_2, l_3, l_4, l_5\}$	–	–	$\{l_6, l_7\}$
N_7	$\{l_1, l_2, l_3, l_4, l_5, l_6\}$	–	–	$\{l_7\}$
N_{PLC}	$\{l_1, l_2, l_3, l_4, l_5, l_6, l_7\}$	–	–	$\varnothing$

4.3. Case Study 2: Multiple ISC Faults on Simple Topology

In this case study, for cases A and B shown in Figure 9, the ISC faults occur independently on two different links, i.e., l_1 and l_5. In total, 3277 error messages are recorded in this case study.

Step 1. Produce Direction Events: Based on the VTDFG for bus topology (13), the types of direction events, as well as the ratio of each type over a total number of records for all nodes can be obtained, as shown in Table 4.

Step 2. Derive Domains: The fault domains and health domains for all nodes can be derived by (9) and (10), respectively, as shown in Table 5.

Step 3. Locate ISC Faults: By using the domains for all nodes obtained from sensor T_1 and (14), the T_1-direction location result is $ISC_{T_1} = \{l_1\} - \varnothing = \{l_1\}$. By using the domains for all nodes obtained from sensor T_2 and (14), the T_2-direction location result is $ISC_{T_2} = \{l_5, l_6, l_7\} - \{l_6, l_7\} = \{l_5\}$. Therefore, the set of ISC fault locations is $ISC_{Network} = ISC_{T_1} \bigcup ISC_{T_2} = \{l_1, l_5\}$, which agrees with the experimental setup.

Table 4. Direction events and corresponding ratio for nodes in case study 2.

N_k	N_1	N_2	N_3	N_4	N_5	N_6	N_7	N_{PLC}
$\mathcal{E}_{T_1}^{N_k}$	0	50.3%	52.2%	52.8%	55.4%	99.6%	99.4%	100%
$\mathcal{E}_{T_2}^{N_k}$	100%	49.7%	47.8%	47.2%	44.6%	0.4%	0.6%	0

Table 5. Fault domains and health domains of direction events in case study 2.

N_k	$\mathcal{FT}_{T_1}^{N_k}$	$\mathcal{HL}_{T_1}^{N_k}$	$\mathcal{FT}_{T_2}^{N_k}$	$\mathcal{HL}_{T_2}^{N_k}$
N_1	–	$\varnothing$	$\{l_1, l_2, l_3, l_4, l_5, l_6, l_7\}$	–
N_2	$\{l_1\}$	–	$\{l_2, l_3, l_4, l_5, l_6, l_7\}$	–
N_3	$\{l_1, l_2\}$	–	$\{l_3, l_4, l_5, l_6, l_7\}$	–
N_4	$\{l_1, l_2, l_3\}$	–	$\{l_4, l_5, l_6, l_7\}$	–
N_5	$\{l_1, l_2, l_3, l_4\}$	–	$\{l_5, l_6, l_7\}$	–
N_6	$\{l_1, l_2, l_3, l_4, l_5\}$	–	–	$\{l_6, l_7\}$
N_7	$\{l_1, l_2, l_3, l_4, l_5, l_6\}$	–	–	$\{l_7\}$
N_{PLC}	$\{l_1, l_2, l_3, l_4, l_5, l_6, l_7\}$	–	–	$\varnothing$

4.4. Case Study 3: ISC Diagnosis for Complex Topology

In this case study, as shown in Figure 10, the ISC faults occur on the link between nodes X_1 and X_2 of branch X, i.e., l_1. In total, 2979 error messages are recorded in this case study.

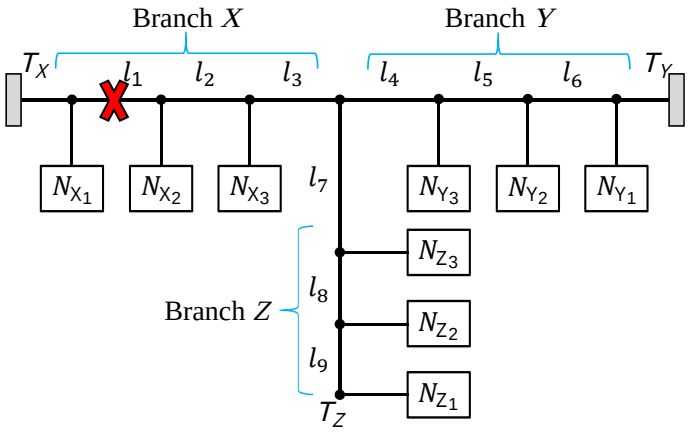


Figure 10. Network topology and fault setup in case study 3. The red cross denotes the ISC fault.

Step 1. Produce Direction Events: Based on the VTDFGs (7) and (8), the types of direction events, as well as the ratio of each type over a total number of records for all nodes, can be obtained, as shown in Table 6.

Step 2. Derive Domains: The fault domains and health domains for all nodes can be derived by (9) and (10), respectively, as shown in Table 7.

Step 3. Locate ISC Faults: By using the domains for all nodes obtained from the main sensor and (11), the T_{main}-direction location result is $ISC_{T_{main}} = \{l_1\} - \{l_5, l_6, l_8, l_9\} = \{l_1\}$. By using the domains for all nodes obtained from the sub-sensor and (11), the T_{sub}-direction location result is $ISC_{T_{sub}} = \{l_1, l_2, l_3, l_4, l_7\} - \{l_2, l_3, l_4, l_5, l_6, l_7, l_8, l_9\} = \{l_1\}$. Therefore, the set of ISC fault locations is $ISC_{Network} = ISC_{T_{main}} \bigcup ISC_{T_{sub}} = \{l_1\}$, which agrees with the experimental setup.

Table 6. Direction events and corresponding ratio for nodes in case study 3.

$N_{\bullet_k}$	N_{X_1}	N_{X_2}	N_{X_3}	N_{Y_1}	N_{Y_2}	N_{Y_3}	N_{Z_1}	N_{Z_2}	N_{Z_3}
$\mathcal{E}^{N_{\bullet_k}}_{T_{main}}$	0	99.2%	99.6%	0	0.6%	0.6%	0	0.9%	0.5%
$\mathcal{E}^{N_{\bullet_k}}_{T_{sub}}$	100%	0.8%	0.4%	100%	99.4%	99.4%	100%	99.1%	99.5%

Table 7. Fault domains and health domains of direction events in case study 3.

$N_{\bullet_k}$	$\mathcal{FT}^{N_{\bullet_k}}_{T_{main}}$	$\mathcal{HL}^{N_{\bullet_k}}_{T_{main}}$	$\mathcal{FT}^{N_{\bullet_k}}_{T_{sub}}$	$\mathcal{HL}^{N_{\bullet_k}}_{T_{sub}}$
N_{X_1}	–	$\varnothing$	$\{l_1, l_2, l_3, l_4, l_5, l_6, l_7, l_8, l_9\}$	–
N_{X_2}	$\{l_1\}$	–	–	$\{l_2, l_3, l_4, l_5, l_6, l_7, l_8, l_9\}$
N_{X_3}	$\{l_1, l_2\}$	–	–	$\{l_3, l_4, l_5, l_6, l_7, l_8, l_9\}$
N_{Y_1}	–	$\varnothing$	$\{l_1, l_2, l_3, l_4, l_5, l_6, l_7, l_8, l_9\}$	–
N_{Y_2}	–	$\{l_6\}$	$\{l_1, l_2, l_3, l_4, l_5, l_7, l_8, l_9\}$	–
N_{Y_3}	–	$\{l_5, l_6\}$	$\{l_1, l_2, l_3, l_4, l_7, l_8, l_9\}$	–
N_{Z_1}	–	$\varnothing$	$\{l_1, l_2, l_3, l_4, l_5, l_6, l_7, l_8, l_9\}$	–
N_{Z_2}	–	$\{l_9\}$	$\{l_1, l_2, l_3, l_4, l_5, l_6, l_7, l_8\}$	–
N_{Z_3}	–	$\{l_8, l_9\}$	$\{l_1, l_2, l_3, l_4, l_5, l_6, l_7\}$	–

5. Discussion

In this section, the robustness and limitations of the method proposed in this work are discussed.

First, in order to verify that the node resistance within the interval specified in ISO 11898-2 [27] does not affect the location result of the proposed method, the VTDF values calculated using the minimum, median, and maximum values of the node resistance interval, respectively, are compared based on the same error messages recorded in case study 1. Figure 11 shows the results for nodes 2 and 7 (the results for other nodes, which are

omitted due to page limitations, show a similar trend), where the upper and lower bounds of the error bars are the positive and negative standard deviations of the VTDF values. It shows that the node resistance does not affect the magnitude relationship between the two VTDF values, which would produce the same direction event table as Table 2 and lead to the same location result.

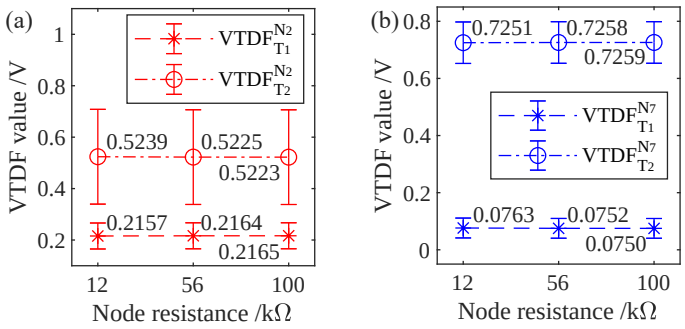


Figure 11. Comparison of the two VTDF values calculated using different node resistances in case study 1. Results for (**a**) node 2 and (**b**) node 7.

Second, the network case where there are nodes in the error-passive state may affect the effectiveness of the method. The DAQ phase of the proposed method is triggered by detecting error flags. However, the error-passive flag (six consecutive recessive bits) from the error-passive node is difficult to detect, because the recessive bits can be easily overwritten by the dominant bits or overlapped with the interframe space that is also consecutive recessive bits. Therefore, the proposed method cannot produce direction events for the error-passive nodes and thus may result in incorrect diagnosis in this particular case. In this work, we assume that all nodes in the network are in the error-active state, as described in Section 2.2.

Third, the fault case where ISC faults occur simultaneously at multiple locations may affect the effectiveness of the method. Because the proposed method only models and analyzes the cases where only one ISC fault occurs at the same moment, the method is likely to produce incorrect direction events due to model errors when the faults at multiple locations occur exactly at the same moment. Nevertheless, as described in the method assumptions in Section 2.2, the probability of multiple faults occurring at the same moment is too low to be negligible.

6. Conclusions

In this paper, a novel ISC fault localization method for the CANs with various topologies is proposed based on two-port network modeling. Voltage transfer difference function groups are derived by using two-port networks to model CAN bus switched systems and ISC faults, based on which the bidirectional eviction localization approach is developed to locate the ISC faults in the network. The testbed is constructed, and three case studies are carried out to demonstrate the effectiveness of the ISC fault localization method. The experimental results show that the ISC fault locations identified by the proposed method agree well with the experimental setups in various topologies and fault location scenarios, including single ISC fault, multiple ISC faults in the bus-topological network, and the ISC fault in the tree-topological network. Moreover, the robustness and the limitations of the proposed method are discussed.

Future work includes improving the current method to localize ISC faults without extracting the specific value of fault voltages and extending the current method to general hybrid IC fault scenarios with both open-circuit and short-circuit IC faults.

Author Contributions: Conceptualization, L.W., Y.Y. and Y.L.; methodology, L.W., Y.Y. and Y.L.; software, L.W. and Y.Y.; validation, L.W.; formal analysis, L.W.; investigation, L.W.; resources, Y.L.; data curation, L.W.; writing—original draft preparation, L.W.; writing—review and editing, L.W. and Y.L.; visualization, L.W.; supervision, Y.L.; project administration, Y.L.; funding acquisition, Y.L. All authors have read and agreed to the published version of the manuscript.

Funding: This study is supported by the National Natural Science Foundation of China under Grant 52072341.

Data Availability Statement: Data is included in the article.

Conflicts of Interest: The authors declare no conflicts of interest.

References

1. Gessner, D.; Barranco, M.; Ballesteros, A.; Proenza, J. sfiCAN: A Star-Based Physical Fault-Injection Infrastructure for CAN Networks. *IEEE Trans. Veh. Technol.* **2014**, *63*, 1335–1349. [CrossRef]
2. Cauffriez, L.; Conrard, B.; Thiriet, J.; Bayart, M. Fieldbuses and their influence on dependability. In Proceedings of the IEEE 20th Instrumentation and Measurement Technology Conference, Vail, CO, USA, 20–22 May 2003; pp. 83–88. [CrossRef]
3. Kelkar, S.; Kamal, R. Adaptive fault diagnosis algorithm for controller area network. *IEEE Trans. Ind. Electron.* **2014**, *61*, 5527–5537. [CrossRef]
4. Yang, Y.; Wang, L.; Li, Z.; Shen, P.; Guan, X.; Xia, W. Anomaly detection for controller area network in braking control system with dynamic ensemble selection. *IEEE Access* **2019**, *7*, 95418–95429. [CrossRef]
5. Wang, Z.; Guo, X.; Yu, C. Research of fault-tolerant redundancy and fault diagnosis technology based on can. In Proceedings of the 2010 2nd International Conference on Advanced Computer Control, Shenyang, China, 27–29 March 2010; Volume 1, pp. 287–291. [CrossRef]
6. Fang, X.; Qu, J.; Tang, Q.; Chai, Y. Intermittent fault recognition of analog circuits in the presence of outliers via density peak clustering with adaptive weighted distance. *IEEE Sens. J.* **2023**, *23*, 13351–13359. [CrossRef]
7. Gouda, B.S.; Panda, M.; Panigrahi, T.; Das, S.; Appasani, B.; Acharya, O.; Zawbaa, H.M.; Kamel, S. Distributed intermittent fault diagnosis in wireless sensor network using likelihood ratio test. *IEEE Access* **2023**, *11*, 6958–6972. [CrossRef]
8. Zhang, K.; Gou, B.; Xiong, W.; Feng, X. An online diagnosis method for sensor intermittent fault based on data-driven model. *IEEE Trans. Power Electron.* **2023**, *38*, 2861–2865. [CrossRef]
9. Huang, C.; Shen, Z.; Zhang, J.; Hou, G. BIT-based intermittent fault diagnosis of analog circuits by improved deep forest classifier. *IEEE Trans. Instrum. Meas.* **2022**, *71*, 3519213. [CrossRef]
10. Yu, M.; Wang, Z.; Wang, H.; Jiang, W.; Zhu, R. Intermittent fault diagnosis and prognosis for steer-by-wire system using composite degradation model. *IEEE J. Emerg. Sel. Top. Circuits Syst.* **2023**, *13*, 557–571. [CrossRef]
11. Farughian, A.; Kumpulainen, L.; Kauhaniemi, K.; Hovila, P. Intermittent earth fault passage indication in compensated distribution networks. *IEEE Access* **2021**, *9*, 45356–45366. [CrossRef]
12. Pohren, D.H.; dos Santos Roque, A.; Kranz, T.A.I.; de Freitas, E.P.; Pereira, C.E. An analysis of the impact of transient faults on the performance of the CAN-FD protocol. *IEEE Trans. Ind. Electron.* **2020**, *67*, 2440–2449. [CrossRef]
13. Roque, A.D.S.; Jazdi, N.; Freitas, E.P.D.; Pereira, C.E. A fault modeling based runtime diagnostic mechanism for vehicular distributed control systems. *IEEE Trans. Intell. Transp. Syst.* **2022**, *23*, 7220–7232. [CrossRef]
14. Zhang, L.; Lei, Y.; Chang, Q. Intermittent connection fault diagnosis for CAN using data link layer information. *IEEE Trans. Ind. Electron.* **2017**, *64*, 2286–2295. [CrossRef]
15. Zhang, L.; Yang, F.; Lei, Y. Tree-based intermittent connection fault diagnosis for controller area network. *IEEE Trans. Veh. Technol.* **2019**, *68*, 9151–9161. [CrossRef]
16. Wang, L.; Hu, S.; Lei, Y. Association Model-Based Intermittent Connection Fault Diagnosis for Controller Area Networks. *Actuators* **2024**, *13* , *358*. [CrossRef]
17. Wang, L.; Zhang, L.; Lei, Y. Diagnosis of intermittent connection faults for CAN networks with complex topology. *IEEE Access* **2023**, *11*, 52199–52213. [CrossRef]
18. Li, T.; Zhao, H.; Zhou, X.; Zhu, S.; Yang, Z.; Yang, H.; Liu, W.; Zhou, Z. Method of Short-Circuit Fault Diagnosis in Transmission Line Based on Deep Learning. *Int. J. Pattern Recognit. Artif. Intell.* **2022**, *36*, 2252009. [CrossRef]
19. Gao, Y.; Zhang, H.; Li, S.; Shi, C.; Gao, H. Short Circuit Fault Location Method of Distribution Network Based on Fuzzy Matching. In Proceedings of the 2022 IEEE 6th Conference on Energy Internet and Energy System Integration (EI2), Chengdu, China, 11–13 November 2022; pp. 1499–1505. [CrossRef]
20. Milhim, A.B.; Ramadhan, H.; Kazemi, H.; Du, X.; Jiang, S.; Sadjadi, H. Voltage-Based Physical Layer Fault Diagnosis for Controller Area Network. In Proceedings of the Annual Conference of the PHM Society, Turin, Italy, 6–8 July 2022; Volume 14. [CrossRef]
21. Krishnamurthy, R.; Bharatiraja, C.; Adedayo, Y.; Tariq, M.; Azeem, A. Locating Wire Fault in Controller Area Network Based on Kelvin (Four-Wire) Resistance Approach. In *Proceedings of the Applications of Computing, Automation and Wireless Systems in Electrical Engineering*; Mishra, S., Sood, Y.R., Tomar, A., Eds.; Springer: Singapore, 2019; pp. 1129–1139.

22. Liwen, W.; Lu, Z.; Meng, X.; Xudong, S. A Fault Diagnosis Scheme for Aircraft Multibranches Wiring Network Based on Matching Algorithm. *Int. J. Distrib. Sens. Netw.* **2015**, *11*, 158364. [CrossRef]
23. Furse, C.; Chung, Y.C.; Lo, C.; Pendayala, P. A critical comparison of reflectometry methods for location of wiring faults. *Smart Struct. Syst.* **2006**, *2*, 25–46. [CrossRef]
24. Gao, Z.; Cecati, C.; Ding, S.X. A Survey of Fault Diagnosis and Fault-Tolerant Techniques—Part I: Fault Diagnosis with Model-Based and Signal-Based Approaches. *IEEE Trans. Ind. Electron.* **2015**, *62*, 3757–3767. [CrossRef]
25. Du, X.; Jiang, S.; Nagose, A.; Zhang, Y.; Wienckowski, N. Locating wire short fault for in-vehicle controller area network with resistance estimation approach. *SAE Int. J. Passeng. Cars—Electron. Electr. Syst.* **2016**, *9*, 93–99. [CrossRef]
26. *ISO 11898-1:2003*; Road Vehicles-Controller Area Network (CAN)—Part 1: Data Link Layer and Physical Signalling. International Organization for Standardization: Geneva, Switzerland, 2003.
27. *ISO 11898-2:2016*; Road Vehicles-Controller Area Network (CAN)—Part 2: High-Speed Medium Access Unit. International Organization for Standardization: Geneva, Switzerland, 2016.
28. Bosch, R. *CAN Specification Version 2.0*; Technical Report; Robert Bosch GmbH: Postfach, Germany, 1991.

Disclaimer/Publisher's Note: The statements, opinions and data contained in all publications are solely those of the individual author(s) and contributor(s) and not of MDPI and/or the editor(s). MDPI and/or the editor(s) disclaim responsibility for any injury to people or property resulting from any ideas, methods, instructions or products referred to in the content.